Nano-Structures & Nano-Objects 17 (2019) 129–137

Contents lists available at ScienceDirect

Nano-Structures & Nano-Objects

journal homepage: www.elsevier.com/locate/nanoso

Effect of confined geometry on the size distribution of nanoparticles produced by laser ablation in liquid medium

Kaushik Choudhury [a], R.K. Singh [a], P. Kumar [b], Mukesh Ranjan [a], Atul Srivastava [c,*], Ajai Kumar [a]

[a] Institute for Plasma Research, Gandhinagar, India
[b] Indian Institute of Science, Bengaluru, India
[c] Indian Institute of Technology Bombay, Mumbai, India

GRAPHICAL ABSTRACT

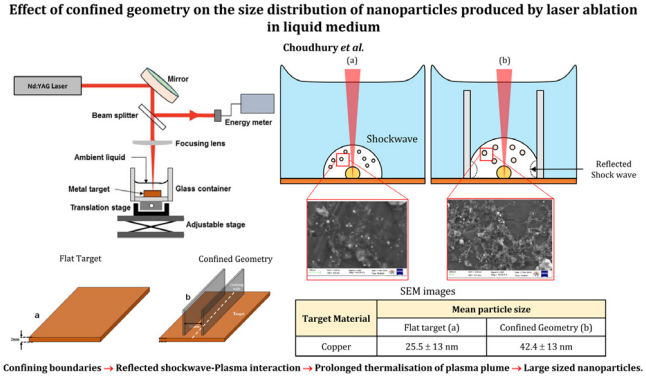

ARTICLE INFO

Article history:
Received 6 September 2018
Received in revised form 3 December 2018
Accepted 22 December 2018

Keywords:
Nanoparticles
Laser ablation in liquids
Plasma plume
Confining boundaries

ABSTRACT

An effective method has been proposed for controlling the size distributions of metallic nanoparticles produced through laser ablation in liquid by employing physical boundaries in the vicinity of the ablation site. An Nd:YAG laser (1064 nm, FWHM 6 ns) has been used to ablate the copper target immersed in two different liquid medium, water and isopropyl alcohol. Water and isopropyl alcohol have been chosen because of the significant differences in their densities while the optical properties are nearly comparable. To demonstrate the efficacy of the method, experiments have been conducted in both the configurations, that is, with and without confining boundaries. To ascertain the observed effect, select experiments have also been carried out with gold as the target material to ensure that the size distribution is not influenced because of oxide-layer formation. The size of the particles were estimated from the SEM images and analysing these images using an indigenously developed code. It has been observed that there are significant differences in the size distributions in the cases of nanoparticles produced with and without confining boundaries. For any given medium, a consistent increase in the mean size of the nanoparticles produced with the targets fitted with physical boundary has been observed as compared to those produced with flat targets. The observed trend has been attributed to the plausible role of the shock wave reflection from the physical boundaries, which alters the plasma parameters. Reflected shock wave–plasma interactions prolonging the thermalisation time of the plasma plume in confined geometry facilitate the particle growth, resulting in the formation of bigger particles. The proposed method, which

* Corresponding author.
E-mail addresses: rajesh@ipr.res.in (R.K. Singh), atulsr@iitb.ac.in (A. Srivastava).

https://doi.org/10.1016/j.nanoso.2018.12.006

can be applied to any metallic target, is one of the greener methods for producing nanoparticles and is also relatively simple and cost effective.

1. Introduction

In recent years, the method of laser ablation has found considerable attention among the researchers as one of the viable methods for the fabrication of nanoparticles. This method has been widely employed for fabricating metallic and polymeric nanoparticles [1–4]. The reason behind the upsurge in the use of this method is that it does not involve any harsh chemicals at any stage of the fabrication process. In addition, it is relatively simpler owing to the absence of any possible chemicals that are otherwise difficult to get rid of once the process of formation of nanoparticles is over [5,6]. Laser ablation can be carried out in air/gas/vacuum or liquid ambient medium based on the desired end results. When laser ablation is carried out in air/gas/vacuum, it is mostly to let the ejected solid get deposited over a substrate, and the method is known as pulsed laser deposition (PLD) [7,8]. On the other hand, when the process of ablation is carried out in liquid, the metal vapour cools down and forms nanoparticles [9–11].

It has been well established through a number of studies that the shape, size and morphology of nanoparticles play an important role in defining their importance in a large range of application areas that include paints, various heat exchange fluids to controlled drug delivery, catalysis and quantum computation [12–15]. Over the last few decades, the area of research has broadened from nanoparticles to nanostructures; encompassing not just spherical or nearly spherical nanoparticles but also a plethora of structures like prisms, cages, spindles, wires etc. [14,16–21]. The variation in the shape, size and/or surface morphology of the nanostructures leads to a change in their physical properties and response to a specific physical, chemical or biological stimulus [17,22–24]. This necessitates achievement of precise control over the shape and size of these nanostructures during their fabrication process itself [25,26]. The parameters that are believed to influence the shape and size of the nanoparticles in the case of chemical synthesis include the concentration of surfactant, choice of precursor, rate of temperature variations etc. [16,24,27–29]. Synthesis of polymeric nanoparticles using wet chemical methods is also a well explored domain and finds applications in the field of biotechnology and life sciences [30,31]. In addition, there are several process-specific parameters that lead to the formation of nanostructures with different shapes and sizes, based on the different mechanisms involved during the fabrication process.

In the context of laser ablation in liquids (LAL), one can choose media with different viscosities, densities, refractive indices etc. in order to control the size of the nanoparticles [32,33]. In some cases, choosing a reactive media also changes the size, size-distribution etc. of the resulting nanoparticles. These different methods have shown the capability of generating a wide range of sizes and size distributions of nanoparticles with different stoichiometry [24,34–39]. Researchers have also shown that parameters like laser wavelength, laser fluence and height of the liquid column also affect the size and size-distribution of the resultant nanoparticles [40,41]. In recent times, some research groups have come with very different and novel methods for controlling the size and the polydispersity of the nanoparticles that are fabricated by LAL. One such method is fabrication of nanoparticles by ablation of thin films fabricated over another substrate. It has been shown that the size of nanoparticles formed depends on the grain size of the material forming the film and also on the thickness of the film [26]. Working on the similar lines, the effect of laser fluence and the effect of cavitation bubble has been reported to be affecting the size and the polydispersity [42]. Also, it has been found that by making layers of thin films and appropriately tailoring the ambient medium, it is possible to achieve core–shell kind of nanostructures of metal alloys [6]. The thickness of shell and composition of the alloy could be altered by changing the thickness of the layers and changing the sequence, for a given liquid ambient [43]. Along these lines, some researchers have altered the thickness and width of the target material to achieve size control. By making the width of the target material smaller or larger than the beam size, different sized nanoparticles have been obtained [44].

Recently, it has been found that the presence of the physical boundaries in the close vicinity of the ablation site causes the reflection of the laser induced shock waves and subsequently affects the medium density and the thermalisation time of the plasma plume [45,46]. With this background we became motivated to explore the influence of physical boundaries on the size and the size distribution of nanoparticles formed by laser ablation in liquid medium. In order to observe the effects of confinement, experiments have been performed with flat metal target and target fitted with confining walls. The produced particles have been characterised for size using scanning electron microscope (SEM) and the observed results have been analysed to understand the effect of confinement. The fact that the proposed methodology of controlling the size distribution of nanoparticles is applicable to any metallic target, is cost effective, simple and is also one of the greener methods, highlights the novelty of the work reported *vis-a-vis* the other conventional methods reported in the literature.

2. Experimental setup

The complete experimental setup employed in the present work has been shown schematically in Fig. 1. An Nd:YAG laser (*Quantel Q-smart* 850, 1064 nm), with a pulse duration of 6 ns, has been used as the ablation beam. The ablation beam has been focused using a converging lens to achieve a spot-size of 0.5 mm at the target surface. A small fraction of the beam was split and let to fall on an optical energy metre to ensure that the laser fluence is constant during the course of the experiments.

Copper and gold plates (99.9% purity), polished and thoroughly rinsed, have been used as the targets. Two different target geometries have been used for both the target materials. The schematics of these two configurations of target plates have been shown in Fig. 2. Fig. 2(a) shows the flat plate target without any physical boundary and Fig. 2(b) shows the target plate fitted with two aluminium confining walls that are 10 mm apart from each other. The walls were screw-fitted on the target. No adhesive has been used so as to avoid any possible contamination. The process of ablation has been carried out in such a way that the point of ablation remains equidistant from both the confining walls. The Al walls were put on the target surface to reflect back the laser-induced shock waves towards the ablation site (plasma plume). Phenomena such as the reflection of laser produced plasma-induced shock waves from the confining boundaries and their characteristics in liquid media of different densities have been studied and reported in detail in our recent articles [45,46].

The LAL experiments have been performed in a custom made glass open-top cuvette of dimensions 60 mm × 60 mm × 60 mm. The chosen dimensions of the cuvette made sure that the total

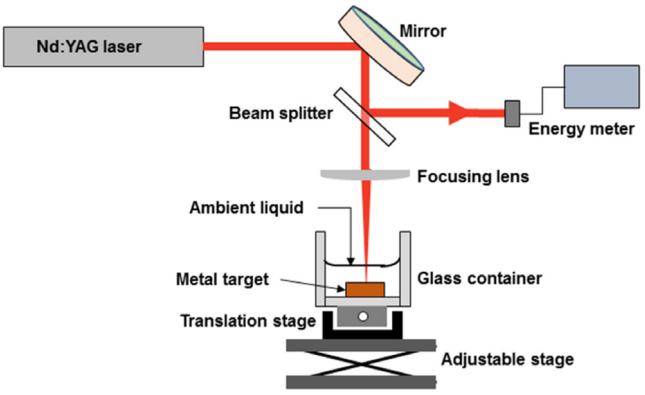

Fig. 1. Schematic diagram of the experimental setup.

travel time of the induced shock waves travelling from the point of ablation to the walls of the container and reflected back to the ablation point is higher than the characteristic thermalisation time of the plasma. This condition needs to be satisfied to avoid any plausible effect of the reflected shock wave in case of the flat plate target geometry. In addition to this, a larger container size was chosen to ensure that the concentration of nanoparticles close to the ablation site is rarified and multiple interactions (of the same particles) with laser are avoided. The ablation chamber has been kept on a translation stage and the target was shifted by 1 mm after every 20 shots to avoid any unwanted effects arising due to the formation of crater or surface modification.

Two sets of experiments (flat and confined target geometry) were performed; one set each with water and isopropyl alcohol (IPA) as the ambient liquids. The reason for selection of IPA and water as the two liquid media has been based on the fact that their densities are significantly different from each other and hence significant contrast in the effect of confinement may be expected. At the same time, the refractive indices of the two liquids differ slightly and hence the transmission and reflection from the liquid target interface do not differ significantly for a chosen target material. It enables us to assume that the laser fluence is constant for the target material in different ambient fluids. In each case, the height of the liquid column was maintained at 10 mm with reference to the top surface of the target surface. Ablation of the target surface has been achieved by firing the laser beam at 5 Hz for 30 min (9000 shots). Considering the height of liquid above the target surface, the energy of the laser was optimised such that maximum amount of ablation took place while the medium did not undergo laser-induced breakdown. This was achieved by setting the laser energy per pulse to a constant value (90 mJ/pulse), which corresponded to the laser fluence of $\sim$11 J/cm^2 on the target surface. This time-span for ablation has been chosen to ensure that there are not too many nanoparticles in the suspension so as to avoid any possibility of agglomeration, as well as, to make sure that the number is high enough to carry out the size characterisation using SEM. Also, the 5 Hz repetition rate was chosen to avoid multiple interaction of nanoparticles with laser-pulse.

3. Materials and methods

Laser ablation in liquid (LAL) has been carried out with copper and gold as the target materials immersed in water and IPA while maintaining constant laser fluence and height of the liquid column. To prepare the samples for SEM characterisation, a few drops of the suspension (carrying ablated nanoparticles) was dried over a cleaned aluminium foil, which was later put on the sample holder using a carbon tape. A Zeiss-Merlin SEM was used which has a resolution of 0.7 nm at 15 kV and 1.2 nm at 1 kV. Before preparing the samples, the suspension was sonicated well to avoid any possibility of agglomeration and ensure homogeneity.

Table 1
Physical properties target materials and ambient liquids.

Refractive index of copper	0.37
Refractive index of water	1.33
Refractive index of IPA	1.35
Reflectivity of water–copper interface	0.310
Reflectivity of IPA–copper interface	0.316
Viscosity of water (at 25 °C)	0.89 cP
Viscosity of IPA (at 25 °C)	2.04 cP
Density of water (at 25 °C)	0.997 g/cm^3
Density of IPA (at 25 °C)	0.786 g/cm^3

The SEM images were later analysed using image processing codes to retrieve the particle size distribution. The images having nanoparticles were processed using image processing toolbox in MATLAB. The step-by-step description of the method has been included in Fig. A.1 in the Appendix and the brief description has been presented here. The images recorded using scanning electron microscopy were processed to enhance the quality of images to enable particle detection through Hough Transform. The images were pre-processed based on the difference in the contrasts between the foreground and background. Here, the foreground is formed by the nanoparticles and background is the substrate onto which nanoparticles were deposited (aluminium foil). Due to the differences in the height among the nanoparticles or nanoparticle clusters with respect to the substrate, there are differences in the intensity values between foreground and the background. Although, the intensity among the nanoparticles has also got some variations, depending upon the size distribution, yet the intensity value for nanoparticles is always greater than the intensity value of the background substrate. These differences in intensity values of substrate and nanoparticles were amplified to enhance the contrast of the image. Thereafter, the images were filtered through top-hat filter. It increased the intensity of brighter pixel with respect to dark background through morphological openings of the image using a structuring element. After, enhancement in the quality of the images, Hough Transform (HT) was applied on the processed images. The parameters were chosen and fine-tuned iteratively to prevent an overestimation or underestimation of diameter and centre of the circle (2D projection of spherical nanoparticles). The diameters of the circle obtained in pixel were converted to real size values through appropriate scaling with scale bar provided on the SEM images.

A detailed discussion on the findings has been made in the next section for the two cases *viz.* the effect of physical boundaries in water ambient and in IPA ambient. The viscosities and densities of water and IPA at 25 °C are significantly different and hence are expected to affect the particle sizes forming due to the process of laser ablation [40]. The refractive indices of the two ambient fluids, however, are close enough to make sure that the amount of laser energy getting reflected from the target–liquid interface is almost same and hence the amount of energy leading to ablation remains unvaried. The values of relevant physical properties have been tabulated below in Table 1 [19,35,38,47].

4. Results and discussion

Primary findings of the present experiments have been discussed in the following sections. Results have been categorised primarily into two different sub-sections. Sections 4.1 and 4.2 include the results of the experiments conducted in water and IPA ambient, respectively. In each of the two sets, experiments were conducted using both the target geometries (flat and confined target).

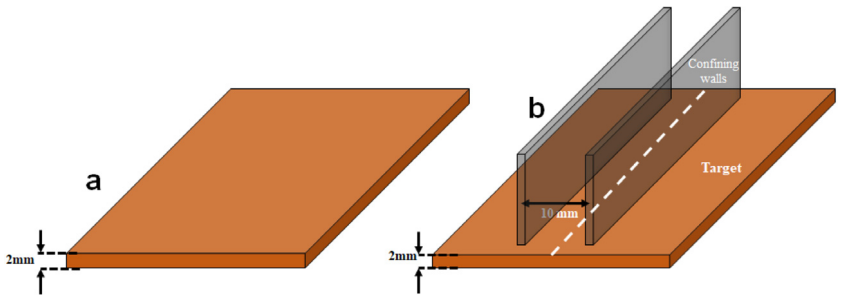

Fig. 2. Schematic representation of the two configurations of the target plate. (a) Flat (open) target and (b) target fitted with confining physical boundaries (Al-wall) on either sides of the ablation site.

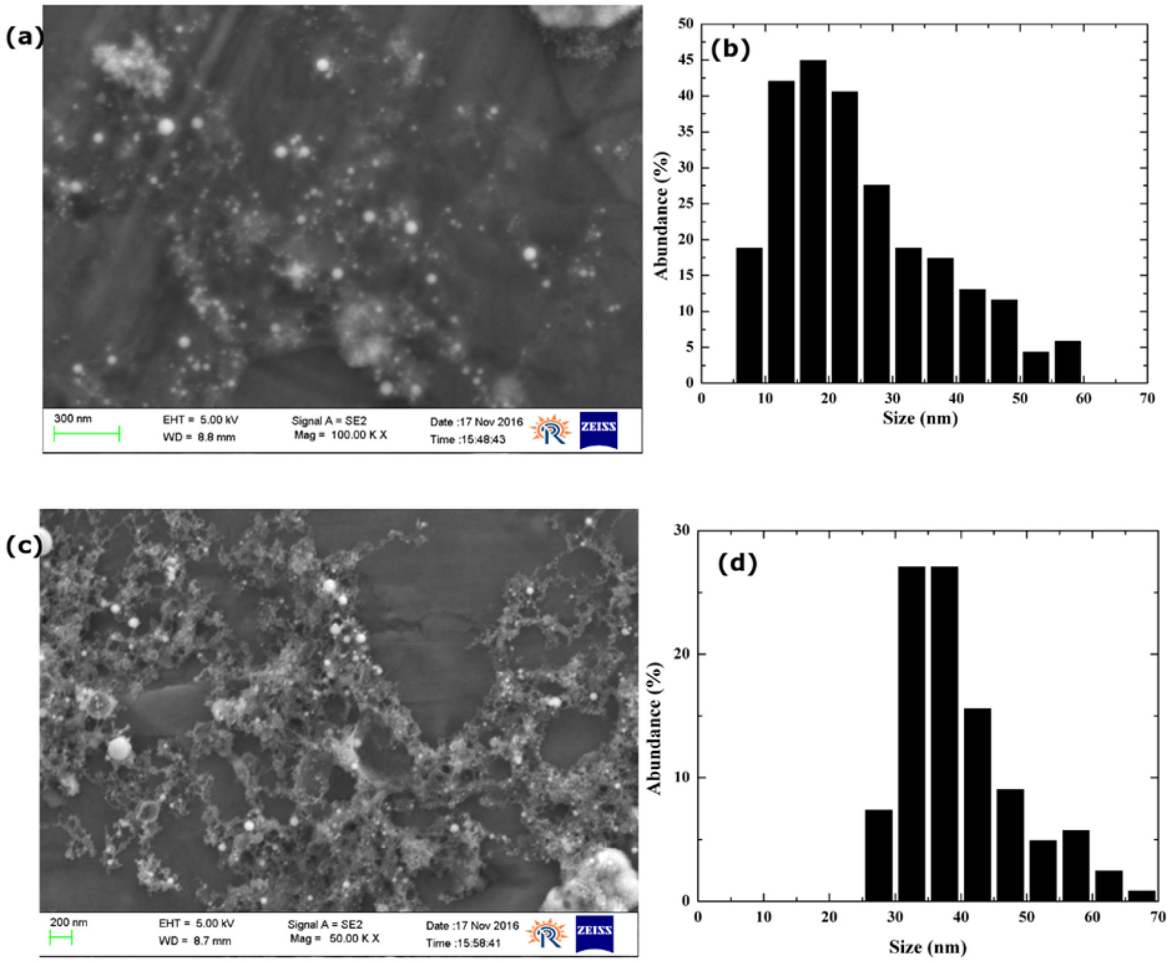

Fig. 3. SEM micrographs of the nanoparticles produced in water ambient as a result of ablation of a flat copper target (a) and copper target fitted with confining physical boundaries (c). Corresponding size-distributions of the resultant nanoparticles have been presented in (b) and (d).

4.1. Experiments in water ambient

As discussed earlier, the size of nanoparticles produced by the method of laser ablation depends on a range of parameters that include laser fluence, ambient medium, physical properties of the target material etc. Effect of many of these parameters on the size distribution of the nanoparticles have been extensively investigated in the past, both, experimentally as well as theoretically [13, 31–34]. In order to see the effect of physical boundary on the size distributions of nanoparticles, energy, wavelength and repetition rate of ablating laser have been maintained constant in the present experiments.

Under these conditions, the laser ablation has been carried out on the target surface that is either flat (no physical barrier) or is confined by the physical boundaries on both the sides of the point of ablation. Following the methodology as discussed in the previous section, samples in the form of suspensions of nanoparticles have been subjected to SEM analysis and the corresponding SEM images have been shown in Fig. 3. Fig. 3a shows the SEM images of the nanoparticles produced due to the ablation of the flat target plate, while the Fig. 3(c) corresponds to the case of target plate with confining walls. Fig. 3(b) and (d) are the corresponding particle size distribution plots. These size-distribution plots clearly highlight the possible influence of the confining boundaries where, the average size of the nanoparticles produced due to the ablation of the flat plate is relatively smaller than that achieved in the case of target surface fitted with physical boundaries. These observations

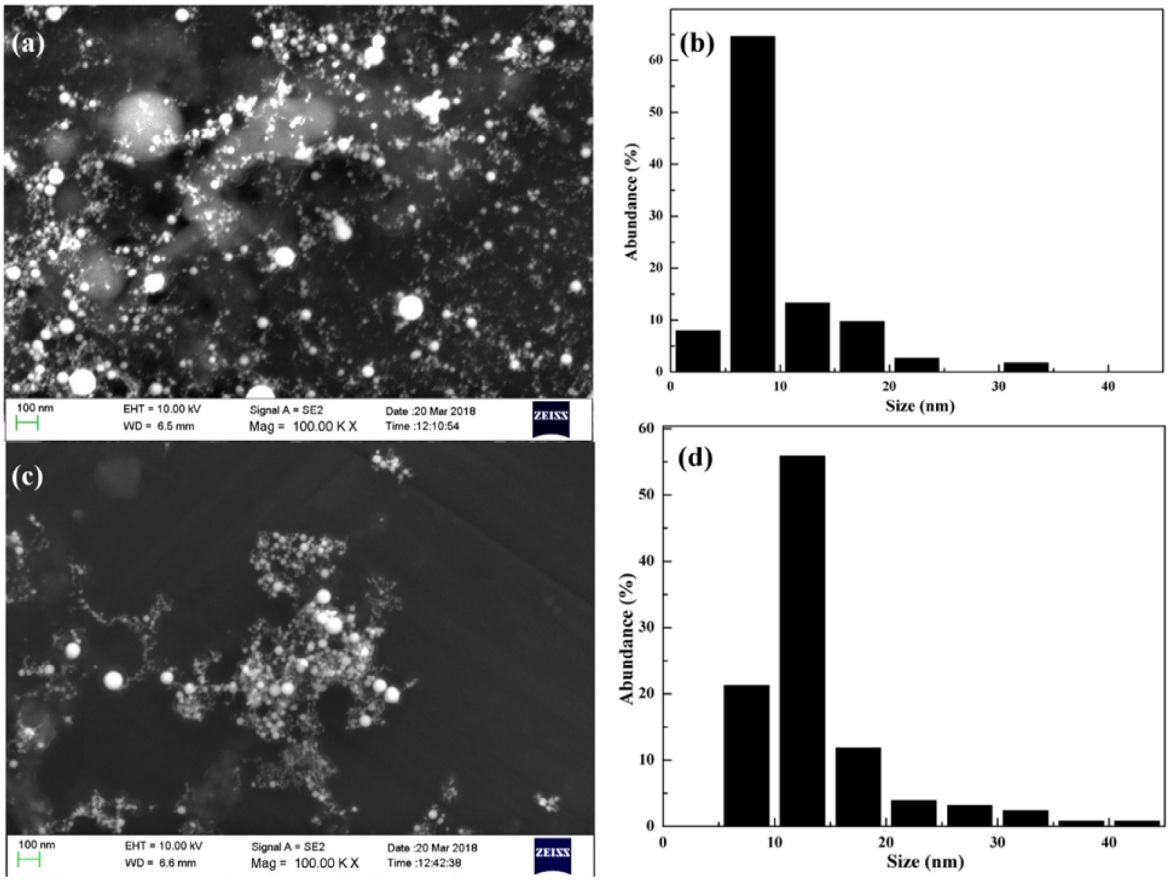

Fig. 4. SEM micrographs of the nanoparticles produced in water ambient as a result of ablation of a flat gold target (a) and gold target fitted with confining physical boundaries (c). Corresponding size-distributions of the resultant nanoparticles have been presented in (b) and (d).

have been quantified in terms of the mean size of the nanoparticles produced with water environment and have been summarised in Table 2. It is to be seen from the table that, the size of the most abundant nanoparticles is higher in the case of the ablation target fitted with the physical boundaries as compared to the case of the flat target. For instance, a percentage increase of nearly 66% in the mean size of the copper-based nanoparticles is to be seen as the flat target is replaced by the one that is fitted with the physical boundaries.

The above observation of the increase in the mean size of nanoparticles in confined geometry may be explained on the basis of thermalisation rate of the plasma plume. It has been reported that the formation of metallic nanoparticles by laser ablation and its size distribution depends on the thermalisation rate of the evolving plasma plume. Thus, the rate at which the plasma plume cools down plays an important role in this entire process [48]. A very high cooling rate of the plasma plume is expected to result into smaller size of the nanoparticles produced. This is owing to the fact that the formation mechanism of nanoparticles after the completion of the ablation process depends on two co-occurring processes, namely, nucleation and particle growth. The nucleation process starts as soon as the ablated species come together, followed by the coalescence of these nuclei that in turn leads to the formation of bigger particles. If the thermalisation is fast enough, the nucleation process dominates, leading to the formation of smaller nanoparticles. On the other hand, if the plume life-time is longer, i.e. if the process of thermalisation takes place over a longer period of time, the nuclei produced as a result of material ablation get enough time to come closer and form bigger particles [35].

Based on the above arguments, the observed result in the present context could be explained as follows: Laser plasma-induced spherical shock front propagates ahead of the plasma plume in the ablation medium. In absence of any confining wall, the energy of the shock wave gets dissipated in the medium. In presence of confining walls, the expanding shock front interacts with the confining wall and gets reflected back and transfers the energy back into the medium (towards the ablation centre). It has been well studied that pressure, density and temperature of the medium increases significantly in the case of the reflected shock wave. Therefore, strengthened reflected shock wave–plasma plume interactions changes the thermo-dynamical properties of the plasma plume in terms of plume heating and thermalisation. Thus, in contrast to the flat target, the presence of confining wall significantly increases the plasma thermalisation time, which causes the enhancement in the sizes of the nano-particles, as illustrated in the figure [27,35].

The experiments performed in water ambient with copper show a definite trend, but there is a probability of formation of copper oxides. Hence, the sizes or size distribution observed may also have a contribution from oxide layers. In order to ensure that oxide formation is not a predominant factor, similar experiments were also performed with gold (99.9% purity) as the target material. The formation of oxide in the case of gold is hardly possible and hence the sizes observed may be considered as the size of the metallic nanoparticles. Therefore, the difference in the sizes of the nanoparticles in the absence and presence of confining walls can purely be attributed to the presence of the physical barriers and the subsequent plasma heating. The results obtained with gold targets ablated under water have been shown in Fig. 4. Fig. 4(a) and (c)

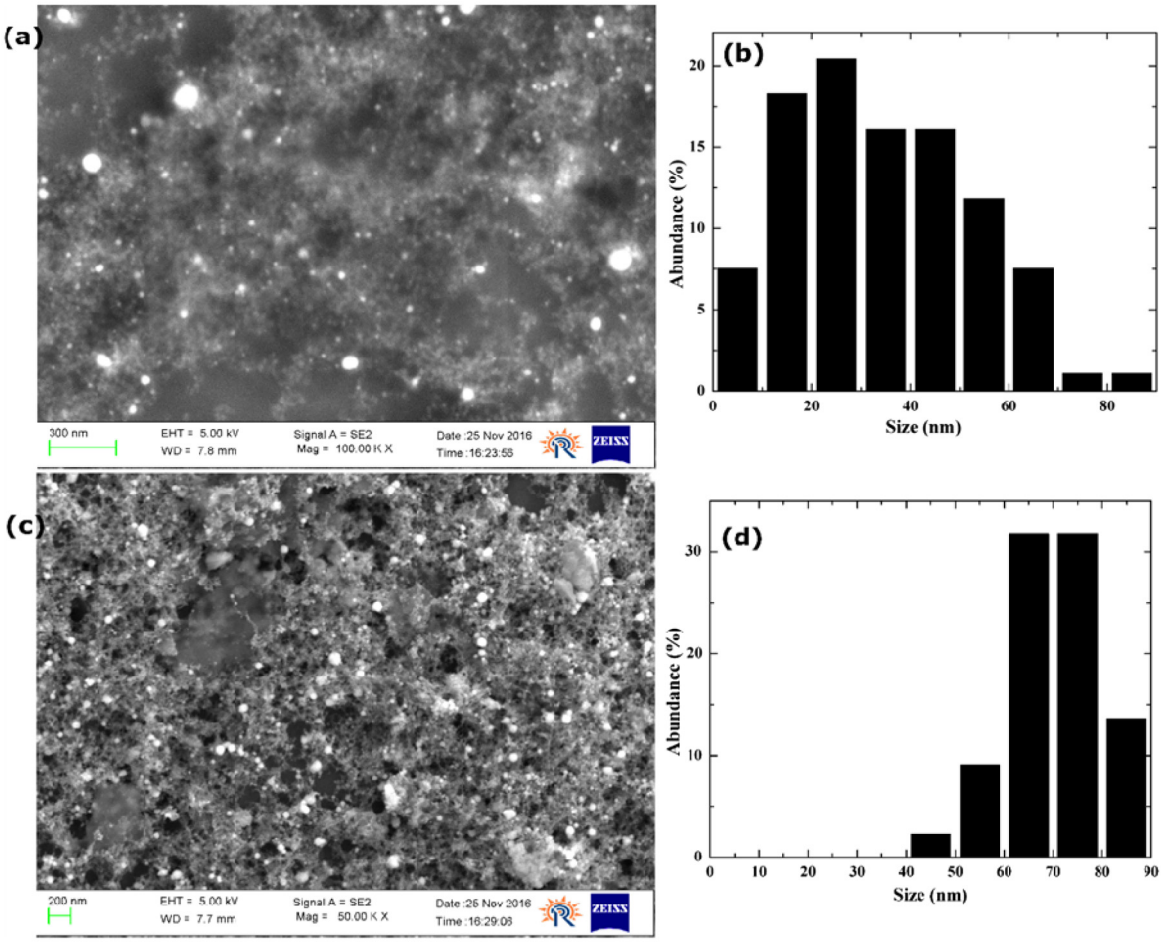

Fig. 5. SEM micrographs of the nanoparticles produced in IPA ambient as a result of ablation of a flat copper target (a) and copper target fitted with confining physical boundaries (c). Corresponding size-distributions of the resultant nanoparticles have been presented in (b) and (d).

Table 2
Comparison of the mean size of the nanoparticles produced with flat target to those obtained with the target fitted with physical boundaries (Ambient liquid medium: Water).

Material	Mean size of nanoparticles		% Increment
	Flat target	Target with boundary	
Copper	25.5 ± 13 nm	42.4 ± 13 nm	66
Gold	9.15 ± 5 nm	13.7 ± 6 nm	49.7

show the SEM images of the gold nanoparticles formed by ablating a flat target and target fitted with walls, respectively. Fig. 4(b) and (d) show the corresponding size distributions.

With reference to the SEM images and corresponding size distributions shown in Fig. 4, it is clearly evident that the size of the gold particles formed in confined geometry is bigger than their counterparts that are produced by ablating a flat target. The quantitative results have been summarised in Table 2. It is, therefore, concluded that prolonged plasma thermalisation due to the presence of physical barrier is primarily responsible for the formation of bigger nanoparticles.

4.2. Experiments in IPA ambient

Observations made on the possible effects of the confining boundaries on the resultant sizes of the nanoparticles produced in isopropyl alcohol (IPA)-based liquid medium have now been presented and discussed. Fig. 5 shows the SEM images and the respective particle size distributions due to the laser ablation of copper target surface immersed in an IPA ambient. Fig. 5(a) and (c) respectively show the SEM images of the nanoparticles formed with flat target (a) and target fitted with physical boundaries (c). The respective particle size distributions of the produced nanoparticles have been shown in Fig. 5(b) and (d). Smaller-sized nanoparticles are to be observed in the case of flat targets while the nanoparticles are relatively bigger in size when produced with confining walls placed on the target surfaces. These results follow the similar trend as was observed in the case of water as the liquid ambient medium presented in the previous section. However, a closer observation of the mean size of the nanoparticles summarised in Table 3 reveals that the copper nanoparticles produced under IPA liquid ambient are relatively larger in size as compared to their counterparts obtained with water as the ambient liquid medium (Row 1 of Table 2). This could be understood as follows: It is a well-studied fact that plasma quenches faster in a dense medium [48]. This is because the plasma plume experiences higher resistive force during its expansion in the denser medium and is confined in a smaller volume. Density of water (0.997 g/cm^3) is significantly higher than the density of IPA (0.786 gm/cm^3), and hence the plasma will quench (thermalise) much faster in water as compared to IPA, resulting in the formation of bigger particles in the IPA ambient. This argument is in-line with the previously presented explanation that the faster thermalisation leads to the formation of smaller particles.

Results of various experiments presented in the above two sections reveal that the changes in the size of the nanoparticles

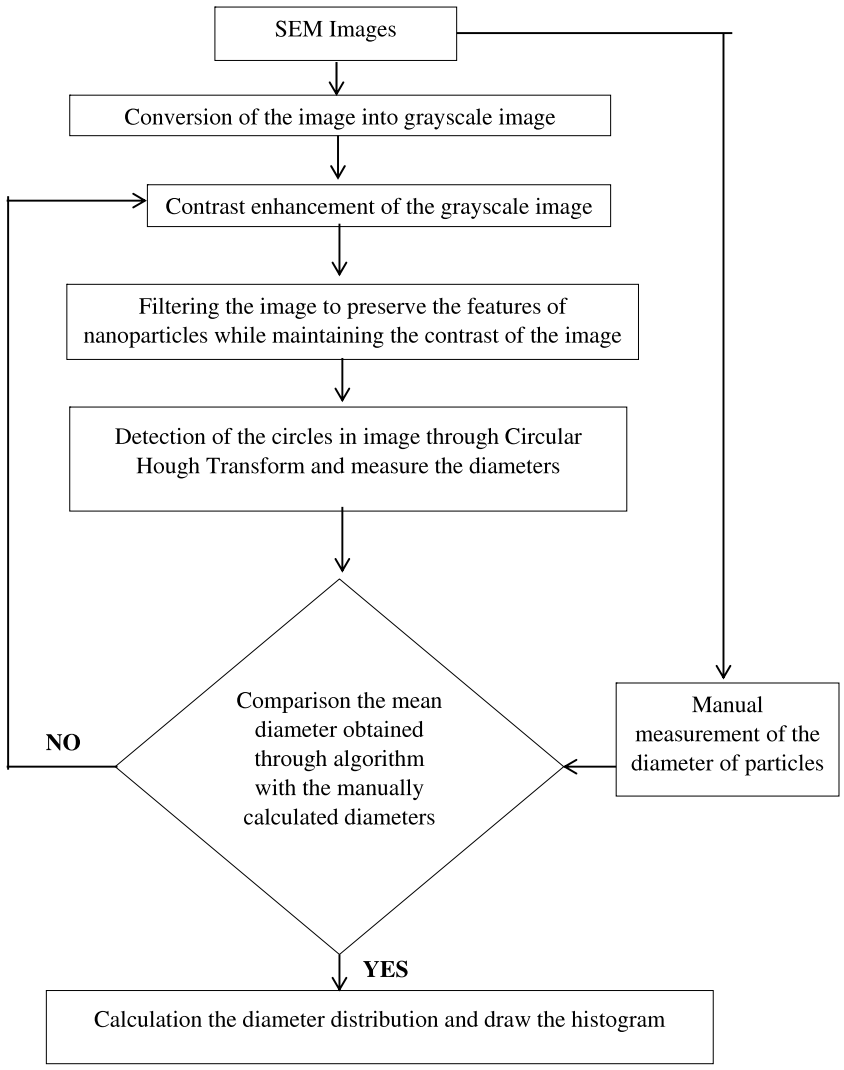

Fig. A.1. Flow-chart of the algorithm employed to extract the sizes of the nanoparticles from the SEM images.

Table 3
Comparison of the mean size of the nanoparticles produced with flat target to those obtained with the target fitted with physical boundaries (Ambient liquid medium: IPA).

Material	Mean size of nanoparticles		% Increment
	Flat target	Target with boundary	
Copper	34.5 ± 18 mm	76.3 ± 17 mm	121

(as one goes from the flat target to the ones fitted with physical boundaries) is significant. These primary findings of the present experimental work have clearly identified the plausible roles of the presence of physical boundaries fitted on either sides of the ablation site in deciding the size and the size distribution of the nanoparticles produced due to the laser ablation of the target material(s) placed in two different liquid media.

5. Conclusions

The plausible control on the size of the nanoparticles produced as a result of ablation of metallic target in a liquid medium using confining boundaries was experimentally demonstrated. An indigenously developed algorithm based on Hough transform has been used to extract the size of the nanoparticles from the SEM images. The experiments revealed that for any given liquid medium, the mean size of the nanoparticles obtained with confining boundaries is consistently higher than that achieved with the flat target materials. It has been observed that the increment in size of the copper nanoparticles in the two cases (bounded and flat) is 66% and 121% in water and IPA ambient, respectively. In order to confirm that the observed sizes of the nanoparticles are not affected because of oxide-layer formation, select set of experiments were also conducted with gold as the target material. The results observed with gold are in agreement with the results obtained with copper target. The observed increase in the size of the nanoparticles in the presence of confining walls was primarily attributed to the interaction of the reflected shock wave and plasma plume leading to the prolonged thermalisation of the plasma plume, which facilitates the growth over the nucleation. Furthermore, the observed difference in the sizes of the particles formed in water and IPA, under similar conditions, has been attributed to the faster quenching of plume in the medium of higher density. The present study demonstrates the proof of concept of the proposed, simple yet effective method, for controlling the size distribution of the nanoparticles formed by laser ablation of metals.

Acknowledgment

The experimental work was partially supported through a BRNS sponsored research grant (Grant No.: 39/14/03/2016-BRNS). The authors acknowledge the support received.

Conflict of interest

The authors declare that they have no known competing financial interests or personal relationships that could have appeared to influence the work reported in this paper.

Appendix

The algorithm used to determine the size of the nanoparticles from the available SEM images has been shown below in the flowchart (see Fig. A.1).

References

[1] M. Ullmann, S.K. Friedlander, A. Schmidt-ott, Nanoparticle formation by laser ablation, 2002, pp. 499–509.

[2] F. Bozon-Verduraz, R. Brayner, V.V. Valerii, N.A. Kirichenko, V.S. Aleksandr, A.S. Georgii, Production of nanoparticles by laser-induced ablation of metals in liquids, Quantum Electron. 33 (2003) 714, http://dx.doi.org/10.1070/QE2003v033n08ABEH002484.

[3] A.H. Lu, E.L. Salabas, F. Schüth, Magnetic nanoparticles: Synthesis, protection, functionalization, and application, Angew. Chem. Int. Ed. 46 (2007) 1222–1244, http://dx.doi.org/10.1002/anie.200602866.

[4] R.F. Cozzens, R.B. Fox, Infrared laser ablation of polymers, Polym. Eng. Sci. 18 (1978) 900–904, http://dx.doi.org/10.1002/pen.760181113.

[5] P. Nancy, J. James, S. Valluvadasan, R.A.V. Kumar, N. Kalarikkal, Laser–plasma driven green synthesis of size controlled silver nanoparticles in ambient liquid, Nano-Struct. Nano-Objects 16 (2018) 337–346, http://dx.doi.org/10.1016/j.nanoso.2018.09.006.

[6] N. Tarasenka, A. Butsen, V. Pankov, T. Velusamy, D. Mariotti, N. Tarasenko, Laser assisted preparation of doped ZnO nanocrystals, Nano-Struct. Nano-Objects 12 (2017) 210–219, http://dx.doi.org/10.1016/j.nanoso.2017.10.008.

[7] R.K. Singh, J. Narayan, Pulsed-laser evaporation technique for deposition of thin films: Physics and theoretical model, Phys. Rev. B 41 (1990) 8843–8859, http://dx.doi.org/10.1103/PhysRevB.41.8843.

[8] M.N.R. Ashfold, F. Claeyssens, G.M. Fuge, S.J. Henley, Pulsed laser ablation and deposition of thin films, 2004, pp. 23–31. http://dx.doi.org/10.1039/b207644f.

[9] G. Compagnini, A.A. Scalisi, O. Puglisi, Production of gold nanoparticles by laser ablation in liquid alkanes, J. Appl. Phys. 94 (2003) 7874–7877, http://dx.doi.org/10.1063/1.1628830.

[10] B. Kumar, R.K. Thareja, Growth of titanium nanoparticles in confined plasma, Phys. Plasmas 19 (2012) 033516, http://dx.doi.org/10.1063/1.3697978.

[11] H. Park, D.A. Reddy, Y. Kim, S. Lee, R. Ma, T.K. Kim, Synthesis of ultra-small palladium nanoparticles deposited on CdS nanorods by pulsed laser ablation in liquid: Role of metal nanocrystal size in the photocatalytic hydrogen production, Chem. A Eur. J. 23 (2017) 13112–13119, http://dx.doi.org/10.1002/chem.201702304.

[12] B. Ankamwar, Biomedical engineering - technical applications in medicine, in: Biomed. Eng. - Tech. Appl. Med., Intech, 2012, pp. 93–114.

[13] T.M. Allen, P.R. Cullis, Drug Delivery Systems : Entering the Mainstream, 10388, 2003.

[14] A. Abbasi, H. Khojasteh, M. Hamadanian, M. Salavati-Niasari, Normal spinel CdCr2O4and CdCr2O4/Ag nanocomposite as novel photocatalysts, for degradation of water contaminates, Sep. Purif. Technol. 195 (2018) 37–49, http://dx.doi.org/10.1016/j.seppur.2017.11.077.

[15] M. Hassanpour, H. Safardoust-Hojaghan, M. Salavati-Niasari, Rapid and eco-friendly synthesis of NiO/ZnO nanocomposite and its application in decolorization of dye, J. Mater. Sci. Mater. Electron. 28 (2017) 10830–10837, http://dx.doi.org/10.1007/s10854-017-6860-3.

[16] L.E. Euliss, J.A. DuPont, S. Gratton, J. DeSimone, Imparting size, shape, and composition control of materials for nanomedicine, Chem. Soc. Rev. 35 (2006) 1095–1104, http://dx.doi.org/10.1039/b600913c.

[17] S. Bhatia, Natural polymer drug delivery systems, in: Nat. Polym. Drug Deliv. Syst., Springer, 2016, pp. 33–93, http://dx.doi.org/10.1007/978-3-319-41129-3.

[18] H. Zeng, X.W. Du, S.C. Singh, S.A. Kulinich, S. Yang, J. He, W. Cai, Nanomaterials via laser ablation/irradiation in liquid: A review, Adv. Funct. Mater. 22 (2012) 1333–1353, http://dx.doi.org/10.1002/adfm.201102295.

[19] Y.-H. Yeh, M.-S. Yeh, Y.-P. Lee, C.-S. Yeh, Formation of Cu nanoparticles from CuO powder by laser ablation in 2-Propanol, Chem. Lett. 27 (1998) 1183.

[20] N. Haustrup, G.M. O & apos; Connor, Nanoparticle generation during laser ablation and laser-induced liquefaction, Phys. Procedia 12 (2011) 46–53, http://dx.doi.org/10.1016/j.phpro.2011.03.104.

[21] G.W. Yang, Laser ablation in liquids: Applications in the synthesis of nanocrystals, Prog. Mater. Sci. 52 (2007) 648–698, http://dx.doi.org/10.1016/j.pmatsci.2006.10.016.

[22] A. Albanese, P.S. Tang, W.C.W. Chan, [Review] The effect of nanoparticle size, shape, and surface chemistry on biological systems, Annu. Rev. Biomed. Eng. 14 (2012) 1–16, http://dx.doi.org/10.1146/annurev-bioeng-071811-150124.

[23] A.A. Alswat, M. Bin Ahmad, M.Z. Hussein, N.A. Ibrahim, T.A. Saleh, Copper oxide nanoparticles-loaded zeolite and its characteristics and antibacterial activities, J. Mater. Sci. Technol. 33 (2017) 889–896, http://dx.doi.org/10.1016/j.jmst.2017.03.015.

[24] H. Park, D.A. Reddy, Y. Kim, S. Lee, R. Ma, M. Lim, T.K. Kim, Hydrogenation of 4-nitrophenol to 4-aminophenol at room temperature: Boosting palladium nanocrystals efficiency by coupling with copper via liquid phase pulsed laser ablation, Appl. Surf. Sci. 401 (2017) 314–322, http://dx.doi.org/10.1016/j.apsusc.2017.01.045.

[25] S. Barcikowski, G. Compagnini, Advanced nanoparticle generation and excitation by lasers in liquids, Phys. Chem. Chem. Phys. 15 (2013) 3022–3026, http://dx.doi.org/10.1039/c2cp90132c.

[26] D.M. Bubb, S.M. O'Malley, J. Schoeffling, R. Jimenez, B. Zinderman, S. Yi, Size control of gold nanoparticles produced by laser ablation of thin films in an aqueous environment, Chem. Phys. Lett. 565 (2013) 65–68, http://dx.doi.org/10.1016/j.cplett.2013.01.002.

[27] H. Zeng, W. Cai, Y. Li, J. Hu, P. Liu, Composition/structural evolution and optical properties of ZnO/Zn nanoparticles by laser ablation in liquid media, J. Phys. Chem. B 109 (2005) 18260–18266, http://dx.doi.org/10.1021/jp052258n.

[28] T.M. Dung Dang, T.T. Tuyet Le, E. Fribourg-Blanc, M. Chien Dang, The influence of solvents and surfactants on the preparation of copper nanoparticles by a chemical reduction method, Adv. Nat. Sci. Nanosci. Nanotechnol. 2 (2011) 025004, http://dx.doi.org/10.1088/2043-6262/2/2/025004.

[29] Z. Lin, L.V. Zhigilei, V. Celli, Electron–phonon coupling and electron heat capacity of metals under conditions of strong electron–phonon nonequilibrium, Phys. Rev. B - Condens. Matter Mater. Phys. 77 (2008) 1–17, http://dx.doi.org/10.1103/PhysRevB.77.075133.

[30] X. Zhang, K. Wang, M. Liu, X. Zhang, L. Tao, Y. Chen, Y. Wei, Polymeric AIE-based nanoprobes for biomedical applications: Recent advances and perspectives, Nanoscale 7 (2015) 11486–11508, http://dx.doi.org/10.1039/c5nr01444a.

[31] R. Jiang, H. Liu, M. Liu, J. Tian, Q. Huang, H. Huang, Y. Wen, Q. yong Cao, X. Zhang, Y. Wei, A facile one-pot Mannich reaction for the construction of fluorescent polymeric nanoparticles with aggregation-induced emission feature and their biological imaging, Mater. Sci. Eng. C 81 (2017) 416–421, http://dx.doi.org/10.1016/j.msec.2017.08.048.

[32] Y. Tamaki, T. Asahi, H. Masuhara, Solvent-dependent size and phase of vanadyl phthalocyanine nanoparticles formed by laser ablation of VOPc crystal-dispersed solution, Japan. J. Appl. Phys. Part 1 Regul. Pap. Short Notes Rev. Pap. 42 (2003) 2725–2729, http://dx.doi.org/10.1143/JJAP.42.2725.

[33] A. Menéndez-Manjón, B.N. Chichkov, S. Barcikowski, Influence of water temperature on the hydrodynamic diameter of gold nanoparticles from laser ablation, J. Phys. Chem. C 114 (2010) 2499–2504, http://dx.doi.org/10.1021/jp909897v.

[34] N. Takada, T. Sasaki, K. Sasaki, Synthesis of crystalline TiN and Si particles by laser ablation in liquid nitrogen, Appl. Phys. A Mater. Sci. Process. 93 (2008) 833–836, http://dx.doi.org/10.1007/s00339-008-4748-z.

[35] J.S. Golightly, A.W. Castleman, Analysis of titanium nanoparticles created by laser irradiation under liquid environment, J. Phys. Chem. B 110 (2006) 19979–19984, http://dx.doi.org/10.1021/jp062123x.

[36] T.A. Saleh, M.M. Al-Shalalfeh, A.A. Al-Saadi, Graphene Dendrimer-stabilized silver nanoparticles for detection of methimazole using surface-enhanced Raman scattering with computational assignment, Sci. Rep. 6 (2016) 32185, http://dx.doi.org/10.1038/srep32185.

[37] T.A. Saleh, M.M. Al-Shalalfeh, A.A. Al-Saadi, Silver loaded graphene as a substrate for sensing 2-thiouracil using surface-enhanced Raman scattering, Sensors Actuators B Chem. 254 (2018) 1110–1117, http://dx.doi.org/10.1016/j.snb.2017.07.179.

[38] R.M. Tilaki, A. Iraji zad, S.M. Mahdavi, Size, composition and optical properties of copper nanoparticles prepared by laser ablation in liquids, Appl. Phys. A 88 (2007) 415–419, http://dx.doi.org/10.1007/s00339-007-4000-2.

[39] D. Werner, S. Hashimoto, Controlling the pulsed-laser-induced size reduction of Au and Ag nanoparticles via changes in the external pressure, laser intensity, and excitation wavelength, Langmuir 29 (2013) 1295–1302, http://dx.doi.org/10.1021/la3046143.

[40] M.H. Mahdieh, B. Fattahi, Effects of water depth and laser pulse numbers on size properties of colloidal nanoparticles prepared by nanosecond pulsed laser ablation in liquid, Appl. Surf. Sci. 75 (2015) 188–196, http://dx.doi.org/10.1016/j.apsusc.2014.12.069.

[41] M.H. Mahdieh, B. Fattahi, Size properties of colloidal nanoparticles produced by nanosecond pulsed laser ablation and studying the effects of liquid medium and laser fluence, Appl. Surf. Sci. 329 (2015) 47–57, http://dx.doi.org/10.1016/j.apsusc.2014.12.069.

[42] J. Tomko, J.J. Naddeo, R. Jimenez, Y. Tan, M. Steiner, J.M. Fitz-Gerald, D.M. Bubb, S.M. O'Malley, Size and polydispersity trends found in gold nanoparticles synthesized by laser ablation in liquids, Phys. Chem. Chem. Phys. 17 (2015) 16327–16333, http://dx.doi.org/10.1039/C5CP01965F.

[43] V. Amendola, S. Scaramuzza, F. Carraro, E. Cattaruzza, Formation of alloy nanoparticles by laser ablation of Au/Fe multilayer films in liquid environment, J. Colloid Interface Sci. 489 (2017) 18–27, http://dx.doi.org/10.1016/j.jcis.2016.10.023.

[44] S. Scaramuzza, M. Zerbetto, V. Amendola, Synthesis of gold nanoparticles in liquid environment by laser ablation with geometrically confined configurations: Insights to improve size control and productivity, J. Phys. Chem. C 120 (2016) 9453–9463, http://dx.doi.org/10.1021/acs.jpcc.6b00161.

[45] K. Choudhury, R.K. Singh, S. Narayan, A. Srivastava, A. Kumar, Time resolved interferometric study of the plasma plume induced shock wave in confined geometry: Two-dimensional mapping of the ambient and plasma density, Phys. Plasmas 23 (2016) 042108, http://dx.doi.org/10.1063/1.4947032.

[46] K. Choudhury, R.K. Singh, Surya, Narayan, Atul Srivastava, Ajai Kumar, Time-resolved whole field investigation of plasma plume-induced shock wave in liquid media of different densities, Appl. Phys. B 123 (2017) 1–15, http://dx.doi.org/10.1007/s00340-017-6740-9.

[47] W.M. Haynes (Ed.), CRC Handbook of Chemistry and Physics, ninetyseventh ed., CRC Press, 2016.

[48] M. Stafe, A. Marcu, N.N. Puscas, Pulsed Laser Ablation of Solids, 2014. http://dx.doi.org/10.1007/978-3-642-40978-3.